

Article

# Torsional Optical Fiber Stress Analysis and Vortex-Induced Vibration Study of Three-Core Submarine Cable

Haotian Tan , Yanpeng Hao \*, Peng Zhang, Qishun Li, Wanxing Tian, Linhao Chen, Lin Yang and Licheng Li

School of Electric Power Engineering, South China University of Technology, Guangzhou 510640, China; 202121016067@mail.scut.edu.cn (H.T.); eplyang@scut.edu.cn (L.Y.)

\* Correspondence: yphao@scut.edu.cn

**Abstract:** Due to current scouring, submarine cables are prone to be exposed, suspended, and even vortex-induced vibration, which is not conducive to the safe operation of the power grid. In this contribution, the finite element simulation model of a 35 kV three-core optical fiber composite submarine cable with a suspended span length of 9.5 m is established. The natural frequency of the model is obtained through modal analysis. Then the vortex-induced vibration is simulated by the fluid–structure coupling method, and the stress distribution and change law of the torsional optical fiber is extracted. The results show that in the submarine cable, there appears to be a beating vibration and locking phenomena respectively, under two flow velocities. The transverse vibration amplitude of the latter increases significantly due to a resonance state. When the flow direction is perpendicular to the submarine cable, the stress distribution of the torsional optical fiber at the initial moment and at the 1/2 T moment of a vibration cycle approximately represents a mirror image relationship. In addition, the frequency of the stress change is the same as the frequency of the vortex-induced vibration, which can judge whether the vortex-induced vibration occurs. Moreover, the vortex-induced vibration range can be determined by the maximum stress change location.

**Keywords:** submarine cable; vortex-induced vibration; fluid–structure coupling simulation; optical fiber



**Citation:** Tan, H.; Hao, Y.; Zhang, P.; Li, Q.; Tian, W.; Chen, L.; Yang, L.; Li, L. Torsional Optical Fiber Stress Analysis and Vortex-Induced Vibration Study of Three-Core Submarine Cable. *J. Mar. Sci. Eng.* **2023**, *11*, 1589. <https://doi.org/10.3390/jmse11081589>

Academic Editor: José António Correia

Received: 24 July 2023

Revised: 12 August 2023

Accepted: 12 August 2023

Published: 14 August 2023



**Copyright:** © 2023 by the authors. Licensee MDPI, Basel, Switzerland. This article is an open access article distributed under the terms and conditions of the Creative Commons Attribution (CC BY) license (<https://creativecommons.org/licenses/by/4.0/>).

## 1. Introduction

Along with the increase in the installed capacity of offshore wind power [1,2], the number of submarine cables has also increased rapidly as the main power transmission equipment of offshore wind power [3]. Until 2019, the total length of global submarine cables exceeds  $1.2 \times 10^6$  km [4]. Compared with the single-core submarine cable, the three-core submarine cable can save laying area and increase transmission capacity, as shown in Figure 1. At the same time, it has the advantage of reducing loss and is widely used for coastal island power supply and offshore wind farm power transmission [5].



**Figure 1.** Optical fiber composite submarine cables.

Submarine cables are usually buried deep under the seabed. However, due to the complex submarine environment and the erosion from ocean currents, the soil around the

submarine cable may continue to decrease, exposing the submarine cable or even suspending it on the seabed [6]. Previous studies have shown that the submarine cable route of the Hainan networking system has been surveyed many times and found that the submarine cable in the Qiongzhou Strait has been exposed or even suspended in many places due to scouring from ocean currents [7,8]. Under the scouring from the constant currents, the suspended submarine cable will form alternating discharge vortexes in the wake area. Then the shedding of the vortex makes the submarine cable subject to a periodic fluid force, causing it to vibrate in the flow and cross-flow directions (perpendicular to the flow direction). This phenomenon of fluid–structure interaction is called vortex-induced vibration [9]. When the vortex shedding frequency is close to the natural frequency of the submarine cable, the vibration in the cross-flow direction will become very significant, that is, it reaches the resonance state [10]. Vortex-induced vibrations can lead to fatigue and friction of submarine cables, which seriously threaten the operational safety of the power system.

Distributed optical fiber sensing technology is usually used for condition monitoring of submarine cables, which has the advantages of long monitoring distances, high precision, real-time monitoring, and so on. It can monitor the temperature, stress, vibration, and sound waves of submarine cables. In 2014, Zhao et al. monitored the 110 kV single-core optical fiber compo-site submarine cable based on the BOTDR (Brillouin optical time domain reflectometer) and obtained the temperature and strain distributions along the cable [11]. In 2018, Lv et al. used the  $\phi$ -OTDR (phase-sensitive optical time domain reflectometer) to monitor the 35 kV three-core optical fiber composite submarine cable and obtain the vibration data along the submarine cable [12]. Therefore, if a dangerous operation state such as a vortex-induced vibration can be found in time through the change in the optical fiber sensing signal, it is of great significance to the operational safety of submarine cables.

Because it is complicated to carry out the vortex-induced vibration experiments of submarine cables, it is more suitable to study the vortex-induced vibration of submarine cables by using a finite element simulation. In 2019, Khodadadian et al. used the multilevel Monte Carlo finite element method for stochastic time-dependent problems, and it noticeably reduced the computational costs [13]. In 2022, Noh and Khodadadian et al. modeled the random distribution of the inclusions/voids in two- and three-dimensional scenarios and considered their effects on the material stiffness locally and globally by using the Monte Carlo finite element method [14]. These studies have significant reference for the finite element theory and displacement analysis of vortex-induced vibration of submarine cables.

Scholars have conducted extensive simulation research on the vortex-induced vibration of cylinder and submarine-suspended span pipelines [15–17]. However, there are few studies on the vortex-induced vibration of submarine cables.

In 2015, Pan et al. used the fluid–structure coupling method to simulate the vortex-induced vibration of the submarine cable in a piggyback configuration [18]. Then the displacement and strain of the submarine cable in a piggyback configuration were obtained. It was found that vortex-induced lift is the leading cause of transverse vibrations in submarine cables. However, the model is relatively simplified, and there is a lack of modeling for the internal structure of the submarine cable. In 2018, Huang et al. established the finite element model of a 500 kV single-core optical fiber composite submarine cable to analyze its vortex-induced vibration characteristics under a periodic wave load and obtained the displacement, stress, strain, center point acceleration, and other information for each layer structure [19]. However, due to the small amplitude of the model, it did not reflect the amplitude characteristics of vortex-induced vibration. In 2022, Lv et al. established the finite element scaled model of a 110 kV optical fiber composite submarine cable based on the model similarity theory [20]. The natural frequency of the model was obtained through modal analysis. The vortex-induced vibration of the scaled model under different flow velocities was studied by the fluid–structure coupling method and information on vibration amplitude, frequency, and vibration mode was obtained. It was found that the transverse amplitude under resonance was much larger than that under non-resonance.

However, there is no modeling of the optical fiber, and the analysis of the mechanical response characteristics of the optical fiber is lacking.

The above research objectives are all single-core submarine cables, and there is a lack of simulation analysis of vortex-induced vibration for three-core submarine cables. At the same time, the above research lacks the analysis of the mechanical response characteristics of the optical fiber when the submarine cable is in vortex-induced vibration, which is unfavorable to the detection of dangerous states, such as vortex-induced vibration, by the distributed optical fiber sensing technology.

Therefore, this paper establishes a finite element model of a 35 kV three-core optical fiber composite submarine cable with a suspension length of 9.5 m based on the actual size. Then the modal analysis method is used to study the natural frequency of the submarine cable model, and the fluid–structure coupling method is used to simulate the vortex-induced vibration of the submarine cable. In addition, the time–frequency characteristics of submarine cable vibration and the stress distribution of the armor layer under vortex-induced vibrations are studied. Moreover, the stress distribution and variation law of torsional optical fiber are analyzed.

## 2. Fluid Mechanics Theory

### 2.1. Lift Coefficient and Drag Coefficient

According to the theory of fluid mechanics, within a certain range of the Reynolds number, when an ocean current with a stable velocity passes through the submarine cable, it will form a stable vortex with alternating discharge. The transverse periodic force formed by the periodic vortex shedding on submarine cable is called lift, and the periodic force formed along the flow direction is called a drag force. Generally, two dimensionless proportional coefficients are used to describe the force on an object in a fluid. The larger the lift coefficient and drag coefficient, the greater the lift and drag force on the object, which can be calculated using the following formula:

$$C_L = \frac{2F_L}{\rho U^2 S} \tag{1}$$

$$C_D = \frac{2F_D}{\rho U^2 S} \tag{2}$$

where  $F_L$  and  $F_D$  are lift and drag force, respectively,  $\rho$  is the fluid density, and  $U$  is the fluid flow velocity. The value of  $S$  is the product of the diameter and length of the submarine cable.

### 2.2. Reynolds Number and Vortex Shedding Frequency

The Reynolds number  $Re$  describing the fluid state is calculated by the following formula:

$$Re = \frac{\rho U D}{\mu} = \frac{U D}{\nu} \tag{3}$$

where  $D$  is the diameter of the submarine cable,  $\mu$  is the dynamic viscosity of the fluid, and  $\nu$  is the kinematic viscosity of the fluid.

The frequency of vortex shedding is usually obtained by the Fourier transform of the lift coefficient time-domain curve, which also has the following relationship:

$$f_n = \frac{S_t U}{D} \tag{4}$$

where  $S_t$  is the Strouhal number, which is used to characterize the relationship between vortex shedding frequency, flow velocity and cylinder diameter in a specific range of Reynolds numbers, and  $S_t$  is constant [21].

### 2.3. Reduced Velocity

When the submarine cable reaches the vortex-induced resonance, the vortex-shedding frequency will be subject to the natural frequency, making its relationship with the Strouhal number disappear. This phenomenon is called locking. At this time, the reduced velocity  $U_r$  is used to describe the vortex-induced vibration, which can be calculated using the following formula:

$$U_r = \frac{U}{Df_0} \tag{5}$$

where  $f_0$  is the natural frequency of the submarine cable. Some researchers showed that the reduced velocity range of the vortex-induced vibration with maximum amplitude is generally  $5 < U_r < 7$  [22,23].

### 3. Fluid–Structure Interaction Simulation Model

In this paper, the fluid–solid coupling simulation model is established and solved based on the finite element simulation software ANSYS. Among them, the fluid domain is based on the Fluent module, and the solid domain is based on the Transient Structural module. They are iteratively solved through the system coupling module.

#### 3.1. Establish the Finite Element Model

In this paper, the HYJYF41-F 35 kV three-core XLPE (cross-linked polyethylene) insulated optical fiber composite submarine cable is an example for the simulation modeling, and its cross-section is shown in Figure 2a. The cable manufacturer is Zhongtian Technology Co., Ltd. (Nanjing, China). As shown in the figure, the structure of submarine cables is very complex. In order to reduce the difficulty of the simulation, the model needs to be reasonably simplified. Firstly, the modeling of thinner structures is ignored, such as copper tape insulation, water-blocking tape, etc. Secondly, according to the principle of a similar combination of material mechanical parameters, the conductor shield, insulation shield, and XLPE insulation are combined into the insulation layer. Then the PE (polyethylene) sheath and PP (polypropylene) lining layer are combined into the filling layer. The simplified submarine cable model consists of seven layers, including a copper conductor, insulation layer, optical fiber, steel wire sheath, filling layer, armor layer, and outer layer, as shown in Figure 2b.

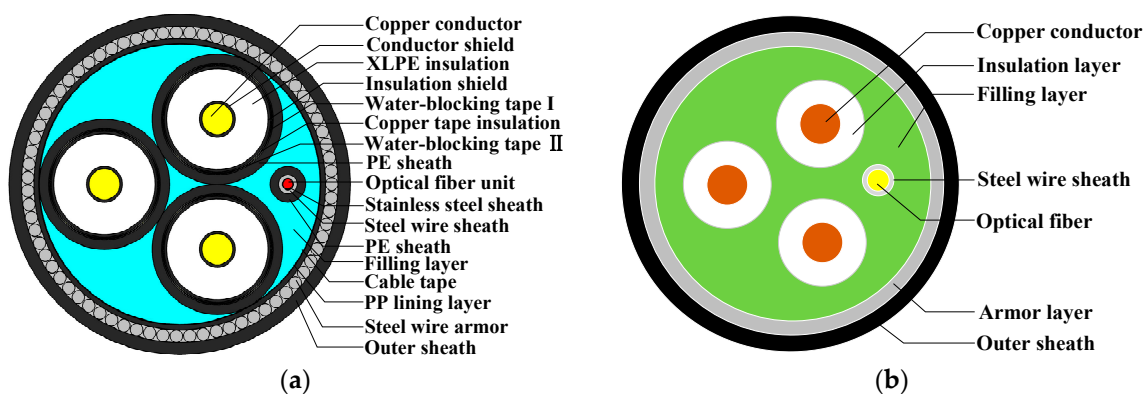


**Figure 2.** Schematic diagram of the cross-section of submarine cable structure: (a) cross-section of the submarine cable; (b) cross-section of the simplified model.

In this paper, the length  $L$  of the submarine cable model is set to 9.5 m, which is five times the torsional pitch of the optical fiber and the diameter  $D$  is 0.109 m. The length  $L$  and diameter  $D$  are used as dimensional parameters to characterize the deformation of the submarine cable at different positions under vortex-induced vibration. The dimensions and material physical parameters of each layer are shown in Tables 1 and 2 [24].

**Table 1.** Structural dimensions of submarine cable.

Component	Thickness (mm)	Outer Diameter (mm)
Copper conductor	—	9.9
Insulation layer	12.1	34.1
Optical fiber	—	3.2
Steel wire sheath	1.4	6
Filling layer	—	93
Armor layer	4	101
Outer sheath	4	109

**Table 2.** Materials physical parameters of the simulation model.

Material	Poisson’s Ratio	Young’s Modulus (Pa)	Density (kg·m <sup>-3</sup> )	Dynamic Viscosity (Pa·s)
Water	—	—	1020	0.001
Copper conductor	0.34	1.26 × 10 <sup>11</sup>	8900	—
Insulation layer	0.41	1.4 × 10 <sup>9</sup>	930	—
Optical fiber	0.27	7.31 × 10 <sup>10</sup>	2203	—
Steel wire sheath	0.3	2 × 10 <sup>11</sup>	7850	—
Filling layer	0.46	3.2 × 10 <sup>8</sup>	946	—
Armor layer	0.3	2 × 10 <sup>11</sup>	7850	—
Outer sheath	0.41	8.9 × 10 <sup>8</sup>	946	—

### 3.2. Boundary Condition

Before solving the fluid–structure coupling model, boundary and initial conditions are set for the simulation model in the fluid and transient structure modules, respectively. The fluid domain is set as a cuboid with a length of 9.5 m, a width of 0.6 m, and a height of 0.6 m. In the fluid domain, inlet, outlet, and no-slip wall boundary conditions are specified. The outlet pressure is set to zero. The fluid–structure interaction interface is defined to enable the transfer of fluid forces from the fluid module to the transient structural module. The above boundary conditions are the Dirichlet boundary condition. Then the flow type is modeled using the SST (shear stress transfer) *k*- $\omega$  turbulence model and gravitational and buoyancy effects are applied to the fluid domain. Specifically, the turbulent intensity is set to 5% and the turbulent viscosity ratio is set to 10. In addition, the flow velocities are set to 1.5 m/s and 2.5 m/s respectively, and the water flow direction is in the X-axis direction, which is perpendicular to the submarine cable. The velocity settings are intended to conduct simulations in both non-resonant and resonant states, facilitating comparative analysis.

To simulate the suspended span state of the submarine cable during vortex-induced vibrations, gravity is applied to the cable model, and fixed supports are set at both ends. Subsequently, the fluid–structure coupling interface is established to transmit the displacement information from the transient structural module to the fluent module. The former is a Dirichlet boundary condition, and the latter is a Neumann boundary condition.

### 3.3. Meshing

The meshing of the fluid and solid domains is performed separately in the fluid module and transient structural module, utilizing linear elements for all mesh cells. The mapping method is used for structured meshing of the fluid domain, and the fluid domain is divided into inner and outer fluid domains. To ensure simulation accuracy while conserving computational resources, the meshing of the inner fluid domain is refined, and boundary layer meshes are created for the fluid–structure interaction interface. Additionally, different meshing methods are applied to various components of the submarine cable model. Both structured and unstructured meshes are used. The torsional structures, such as the copper conductor, insulation layer, optical fiber, and steel sheath, are meshed by the sweeping method. Then the steel wire armor layer and the outer sheath are meshed by the mapping method. Finally, the filler layer is meshed by the patch-conforming method. Among them,

the numbers of tetrahedral meshes, pyramid meshes, hexahedral meshes, and wedge meshes are 1,509,350, 135,427, 289,004 and 11,006 respectively. The final division effect is shown in Figure 3.

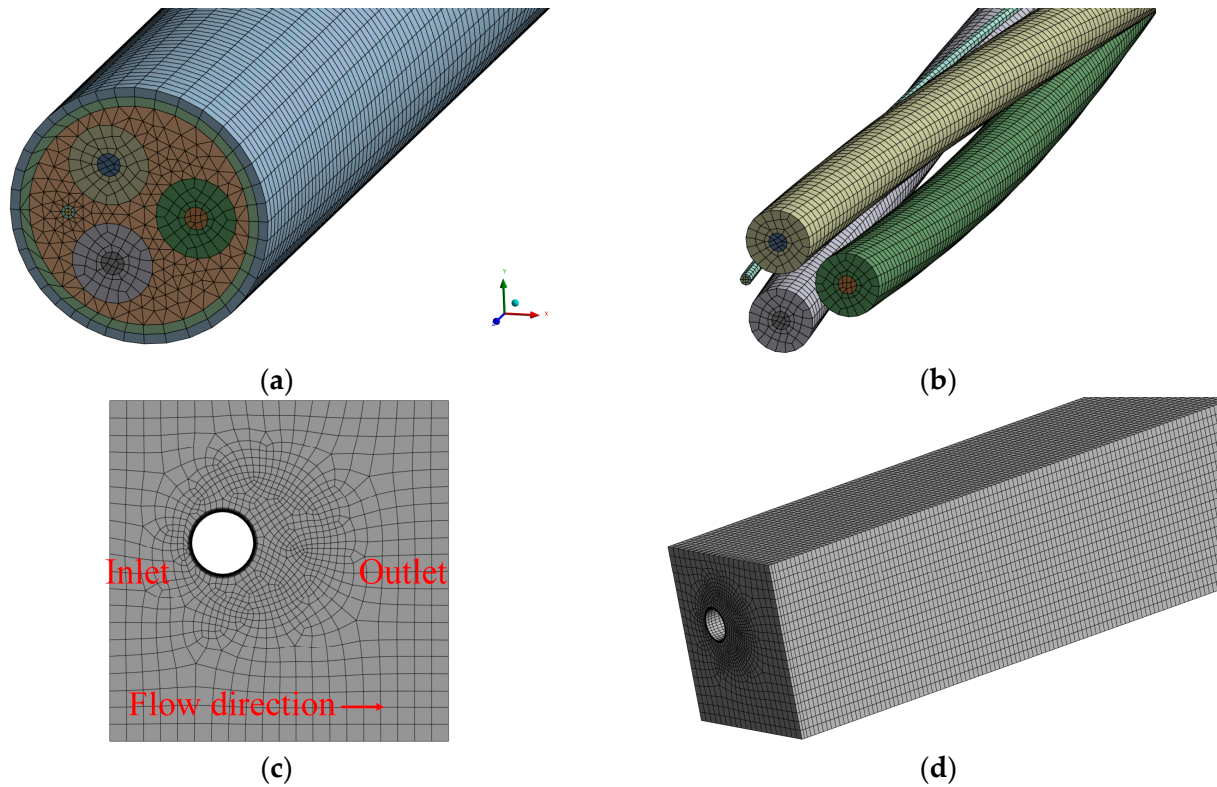


**Figure 3.** Schematic diagram of mesh: (a) meshing of the submarine cable model; (b) meshing of the torsional structure; (c) meshing of the fluid domain cross-section; (d) meshing of the fluid domain.

### 3.4. Governing Equations

The fluid–solid coupling simulation is based on the conservation equations of the fluid field, the equations of the solid field, the basic equations of transient dynamics, and the boundary conditions on the fluid–solid coupling boundary [25,26].

The mass conservation equation and momentum conservation equation of the fluid can be written as follows:

$$\frac{\partial \rho_f}{\partial t} + \nabla \cdot (\rho_f v) = 0 \tag{6}$$

$$\frac{\partial \rho_f v}{\partial t} + \nabla \cdot (\rho_f v v) = \rho_f g + \nabla \cdot \tau \tag{7}$$

where  $\rho_f$  is the fluid density,  $v$  is the fluid velocity vector,  $\tau$  is the stress tensor,  $g$  is the gravitational acceleration vector, and  $t$  is the time.

The equations of the solid field and the basic equations of transient dynamics can be written as follows:

$$\rho_s \ddot{d}_s = \nabla \cdot \sigma_s + f_s \tag{8}$$

$$[M]\{\ddot{u}\} + [C]\{\dot{u}\} + [K]\{u\} = \{F(t)\} \tag{9}$$

where  $\rho_s$  is the fluid density,  $f_s$  is the body force vector,  $\sigma_s$  is the Cauchy stress tensor,  $\ddot{d}_s$  is the acceleration vector,  $[M]$  is the mass matrix,  $[C]$  is the damping matrix,  $[K]$  is the stiffness matrix,  $\{\ddot{u}\}$  is the nodal acceleration vector,  $\{\dot{u}\}$  is the nodal velocity vector,  $\{u\}$  is the nodal displacement vector, and  $\{F(t)\}$  is the load vector.

The boundary conditions on the fluid–solid coupling boundary can be written as follows:

$$\begin{cases} \tau_f \cdot n_f = \tau_s \cdot n_s \\ d_f = d_s \end{cases} \quad (10)$$

where  $\tau_f$  and  $\tau_s$  are the stress tensor of the fluid and solid,  $n_f$  and  $n_s$  is the normal vector, and  $d_f$  and  $d_s$  are the displacement of the fluid and solid.

### 3.5. Coupled Solution

The model is solved by an iterative method, and the governing equations in the fluid–structure interaction model are decoupled equations. In each iterative step, the fluid dynamics equations and solid mechanics equations are solved separately and then interactively updated with each other through an iterative process.

Considering that the submarine cable will have a large displacement, the solution step size of the fluid–structure interaction model is set to 0.002 s. Therefore, the implicit time integration method is set to linearize and solve the fluid–solid coupling equation to ensure the stability and accuracy of the numerical solution.

## 4. Simulation Analysis

Based on the fluid–structure coupling finite element model established above, the wet modal analysis of the 35 kV three-core submarine cable model is carried out first to obtain the natural frequency of the submarine cable model. Subsequently, the fluid–structure coupling simulation is carried out to study the time–frequency characteristics of fluid flow and solid vibration during vortex-induced vibration of the submarine cable. Finally, the mechanical response characteristics of the armor layer and optical fiber are analyzed.

### 4.1. Natural Frequency Calculation

Modal analysis is a general method used to study the dynamic characteristics of mechanical structures. Modal refers to the natural vibration characteristics of mechanical structures. Each mode of a mechanical structure has its corresponding natural frequency and mode shape. Wet modal analysis is the modal analysis of structures in a liquid environment. In this paper, the modal acoustic module is used to analyze the wet mode of the model, thereby obtaining its natural frequencies and mode shapes.

### 4.2. Fluid–Structure Coupling Analysis

#### 4.2.1. Fluid Domain Analysis

The XY plane is set in the middle of the fluid domain to obtain the vortex nephogram of the submarine cable during vortex-induced vibration, which is used to observe the characteristics of fluid changes. At the same time, the lift coefficient curve is set in the output report of the fluid module.

#### 4.2.2. Solid Domain Analysis

In order to analyze the time–frequency characteristics of the submarine cable during vortex-induced vibration, the transverse amplitude at different times is extracted to plot the amplitude time-domain curve and analyze the vortex-induced vibration frequency. At the same time, the deformation nephogram of the submarine cable is extracted to observe the overall displacement and vibration mode of the model. In addition, the sampling path is set to obtain the axial displacement distribution of the submarine cable.

#### 4.2.3. Mechanical Response Analysis of Vortex-Induced Vibration

To visually observe the mechanical response characteristics of the submarine cable under vortex-induced vibration, the stress nephogram is extracted from the armor layer bearing the maximum stress to observe the overall stress distribution. At the same time, sampling paths

are set at different locations along the armor layer to plot the axial stress distribution curves and analyze the stress variations under different flow velocities and positions.

#### 4.3. Torsional Optical Fiber Stress Analysis

In this study, the vibration cycle is set from when the transverse amplitude of the submarine cable reaches its positive peak value to the next time it reaches its positive peak value. To investigate the stress distribution and its development law of the torsional optical fiber during vortex-induced vibration in the submarine cable, the stress along the torsional optical fiber at different times is extracted, and the fiber length–time–stress distribution curve is plotted.

### 5. Results and Discussion

#### 5.1. Natural Frequency Calculation Results

The wet modal analysis of the submarine cable model is carried out through the modal acoustic module, and the results are shown in Table 3. According to the table, the natural frequencies of modes one to six of the submarine cable model fall within the range of 0 to 25 Hz, and the modal shapes exhibit symmetry about the central position. Specifically, the first and second modes exhibit peak amplitudes at the central position, while the third and fourth modes exhibit peak amplitudes at  $1/4 L$  and  $3/4 L$ , respectively. As well as the fifth and sixth modes exhibit peak amplitudes at  $1/6 L$ ,  $1/2 L$ , and  $5/6 L$ .

**Table 3.** Wet modal analysis results of Submarine cable model.

Modal	Natural Frequency (Hz)	Modal
1	4.08	
2	4.09	
3	11.23	
4	11.26	
5	22.02	
6	22.07	

#### 5.2. Analysis of Fluid–Structure Interaction Results

##### 5.2.1. Fluid Domain Simulation Results

According to the fluid–structure interaction simulation results, the vortex discharge nephograms at different times under the two flow velocities are shown in Figure 4. It can be seen from the figure that in the process of vortex discharge, the flow velocity on the upper and lower surfaces of the submarine cable is large. When the velocity is 1.5 m/s, the vortex discharge is relatively smooth, and when the velocity is 2.5 m/s, the vortex discharge is more rapid, and the wake flow becomes unstable.

To study the frequency of vortex discharge at different flow velocities, Fourier analysis was performed on the lift coefficient curve obtained from the calculation results, and the frequency distribution is shown in Figure 5. Since the lift coefficient itself is a dimensionless parameter, the amplitude in Figure 5 has no unit. It can be seen from the figure that the frequency of the lift coefficient exhibits a maximum peak at about 5.86 Hz for a velocity of 2.5 m/s. When the flow velocity is 1.5 m/s, the phenomenon of beat vibration appears [27] and the frequency peaks are 2.44 Hz and 3.42 Hz, respectively. It shows that the frequencies of vortex-induced lift acting on the submarine cable are 5.86 Hz, 2.44 Hz, and 3.42 Hz.

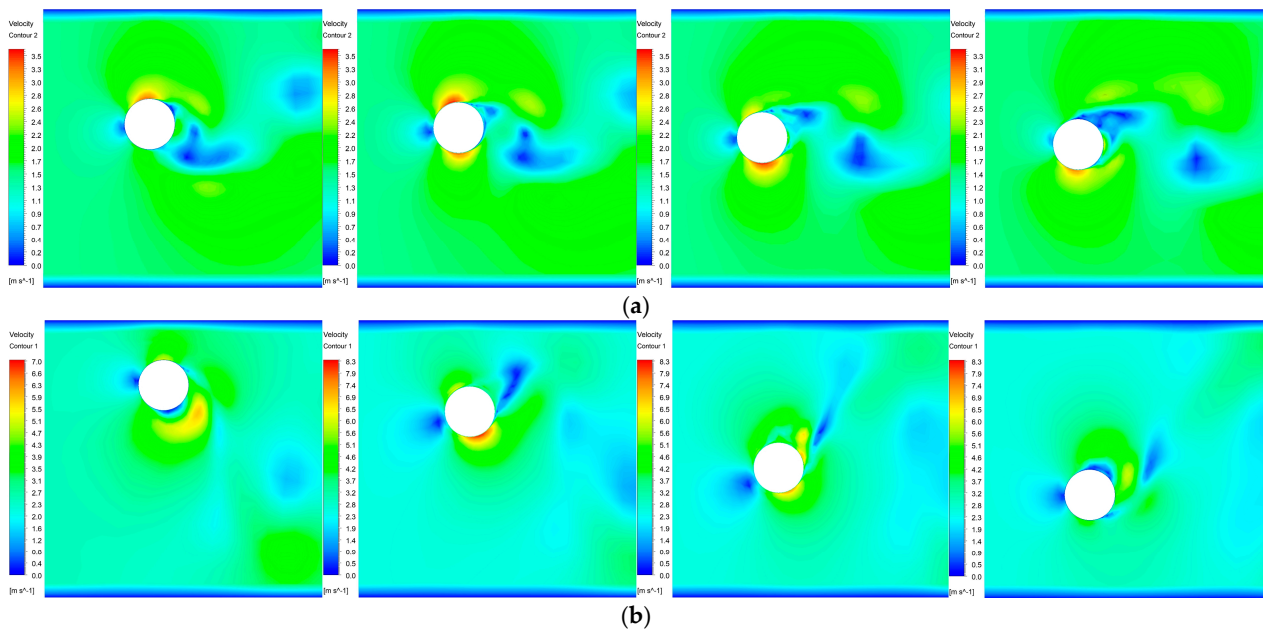


**Figure 4.** Nephogram of vortex discharge at the middle section of 9.5 m submarine cable under different flow velocities: (a) 1.5 m/s; and (b) 2.5 m/s.

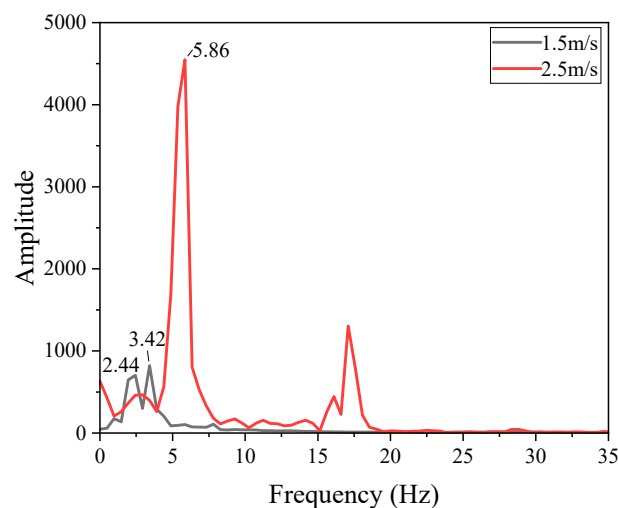


**Figure 5.** Frequency domain analysis of lift coefficient under different flow velocities.

### 5.2.2. Solid Domain Simulation Results

To observe the displacement distribution, the total displacement distribution nephogram of the vortex-induced vibration of the submarine cable model is extracted as shown in Figure 6a,b. From the figure, it can be observed that under the action of water flow with velocities of 1.5 m/s and 2.5 m/s, the submarine cable is displaced due to vortex-induced vibration. Specifically, the displacements are symmetrically distributed about the middle position, which is similar to the first and second-mode shapes.

Moreover, the displacement distribution curve of the submarine cable along the axial direction at a certain moment is shown in Figure 6c. It can be seen from the figure that the displacement along the length of the submarine cable increases first and then decreases at the velocities of 1.5 m/s and 2.5 m/s, and the displacement in the middle is the largest and symmetrically distributed. Specifically, the maximum total displacement is about 0.376 D and the reduced velocity is 3.37 at the flow velocity of 1.5 m/s. When the flow velocity reaches 2.5 m/s, the reduced velocity is 5.62, and a locking phenomenon occurs with a larger displacement, resulting in a maximum total displacement of approximately 1.187 D.

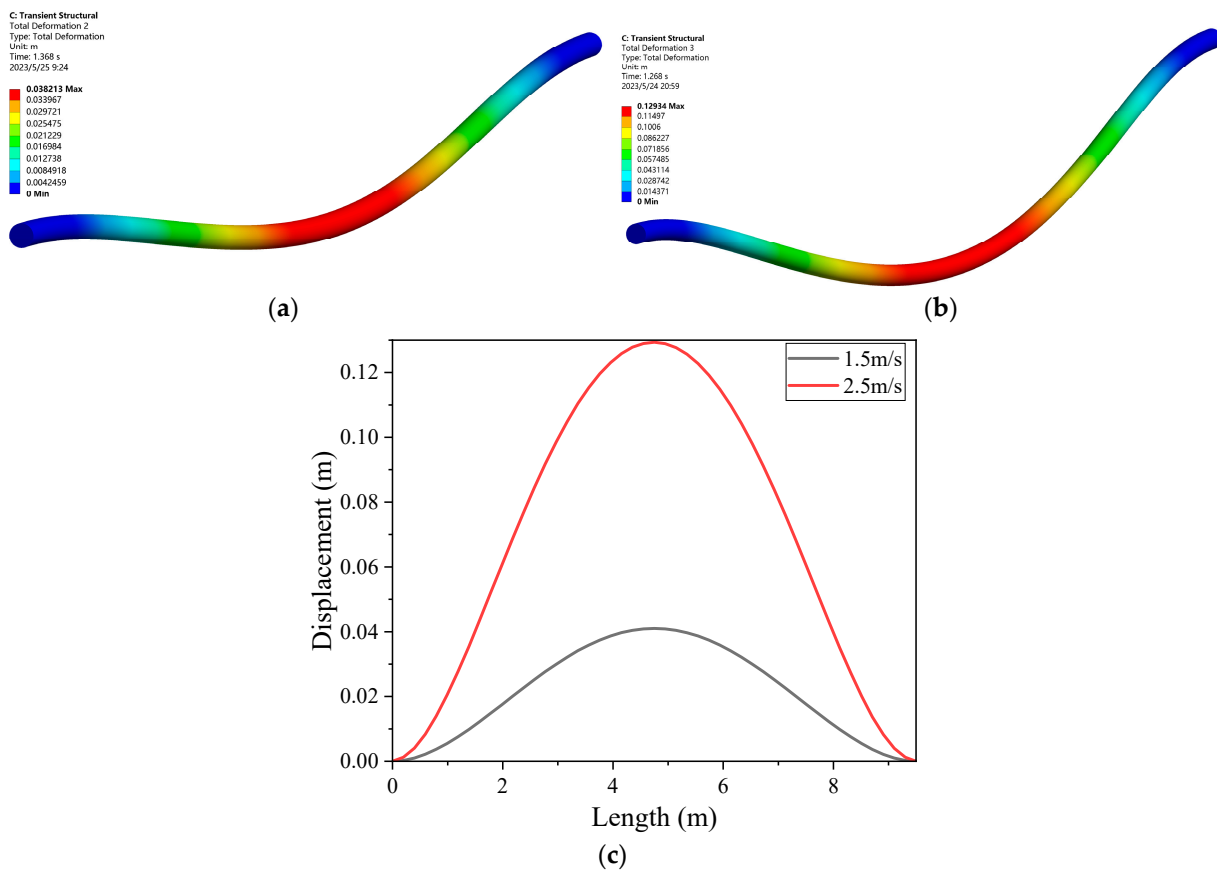


**Figure 6.** Vortex-induced vibration displacement distribution of 35 kV three-core XLPE insulated optical fiber composite submarine cable: (a) vortex-induced vibration displacement nephogram at 1.6 m/s, (b) vortex-induced vibration displacement nephogram at 4.4 m/s, and (c) displacement along the length at different flow velocities.

The time-domain curves of the transverse vibration amplitude for the submarine cable model for flow velocities of 1.5 m/s and 2.5 m/s are extracted and shown in Figure 7a. It can be observed that the transverse vibration amplitude at the flow velocity of 1.5 m/s exhibits no apparent regularity over time. However, due to the gravity being greater than the vortex-induced lift, the transverse vibration amplitude at this velocity is primarily negative, with a maximum amplitude of 0.375 D. In addition, at the velocity of 2.5 m/s, the transverse vibration amplitude of the submarine cable model increases first and then stabilizes gradually with time. Under the action of gravity, the positive peak is slightly smaller than the negative peak, and the maximum vibration amplitude is 1.156 D. Comparing the variation amplitudes at the two flow velocities, it can be noted that the submarine cable model at the velocity of 2.5 m/s reaches the state of vortex-induced resonance, resulting in a locking phenomenon and a sharp increase in transverse amplitude. Therefore, vortex-induced vibration significantly affects the submarine cable in the transverse direction.

By performing Fourier analysis on the transverse vibration amplitude curve, the vortex-induced vibration frequencies at flow velocities of 1.5 m/s and 2.5 m/s are obtained, which are shown in Figure 7b. Among them, the vortex-induced vibration frequency of the submarine cable at the flow velocity of 2.5 m/s is 5.86 Hz. In addition, the beat vibration phenomenon of the submarine cable appears at the velocity of 1.5 m/s, which is composed of two vibrations with similar frequencies. Moreover, the vibration amplitude increases and decreases periodically with time, and the frequencies are 2.44 Hz and 3.42 Hz. Above all, the results of the frequency domain analysis in the solid domain are consistent with those in the fluid domain and are also close to the first and second natural frequencies of the submarine cable model.

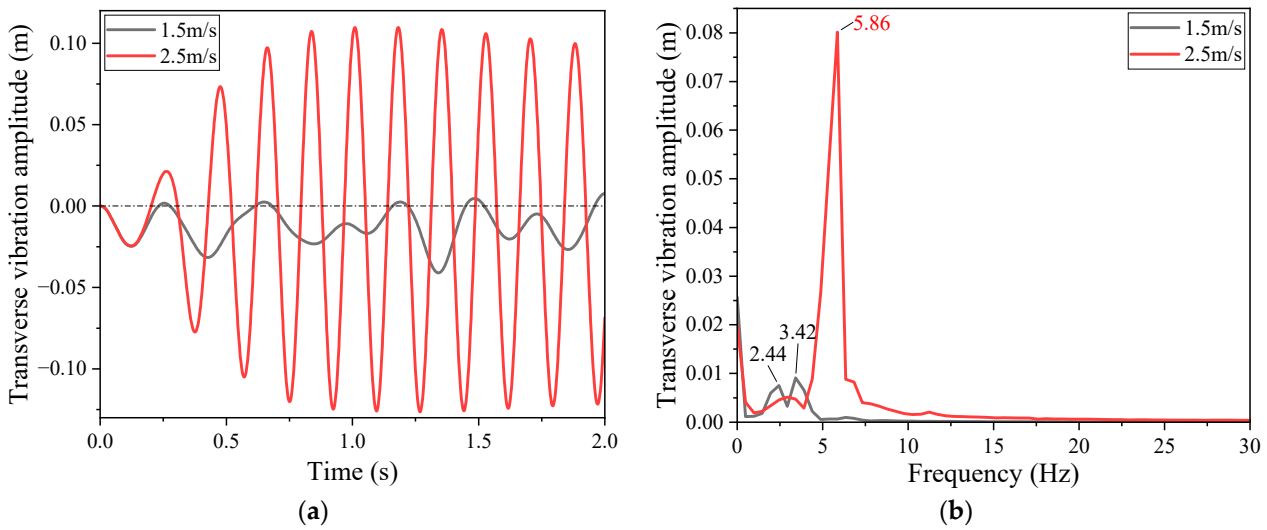


**Figure 7.** Time–frequency characteristics of transverse vibration amplitude of submarine cable under different flow velocities: (a) time domain curve, and (b) frequency domain curve.

5.2.3. Simulation Results of Mechanical Response Characteristics of Vortex-Induced Vibration

In order to analyze the mechanical response characteristics of the submarine cable under vortex-induced vibration, the stress of the armor layer when the transverse amplitude reaches the negative peak is selected for analysis in this section. The stress used in this section is equivalent stress (von-Mises). As seen from Figure 8a,b, the stress distribution of the armor layer under different flow velocities is similar. Both the upper and lower surfaces of the suspension span bear the maximum stress and the middle displacement also bears more stress, which is generally symmetrical. Moreover, the maximum stress of the armor layer at the velocity of 1.5 m/s and 2.5 m/s are 153 MPa and 673 MPa, respectively. It shows that the greater the flow velocity, the greater the mechanical stress on the armor layer. Comparing the strengths of the armor layer, it can be seen that the maximum strain can reach about 3365  $\mu\epsilon$ .

Furthermore, the stress distribution curves of the armor layer at different flow velocities are extracted along sampling paths. It can be seen from Figure 8c that the armor layer bears the maximum stress at the suspension points at both ends of the submarine cable, and the middle position also has a smaller peak stress due to the maximum displacement.

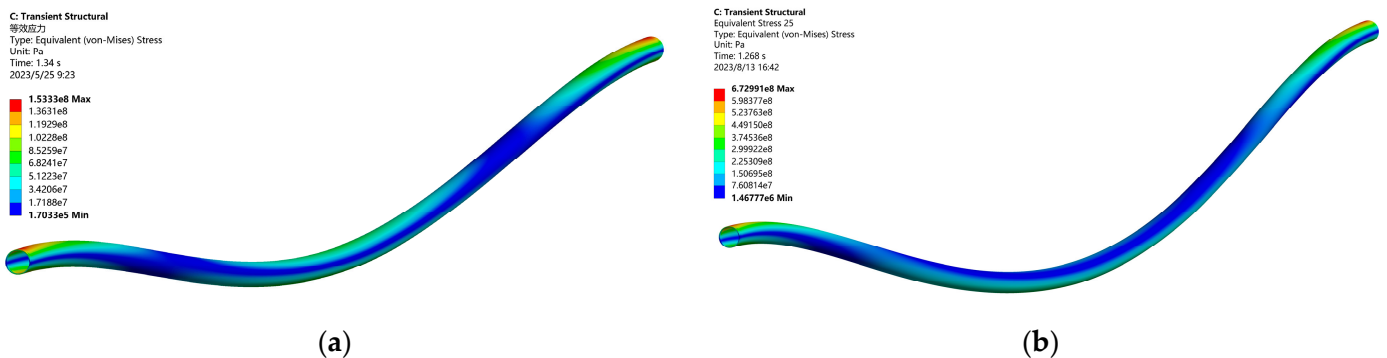


**Figure 8.** Cont.

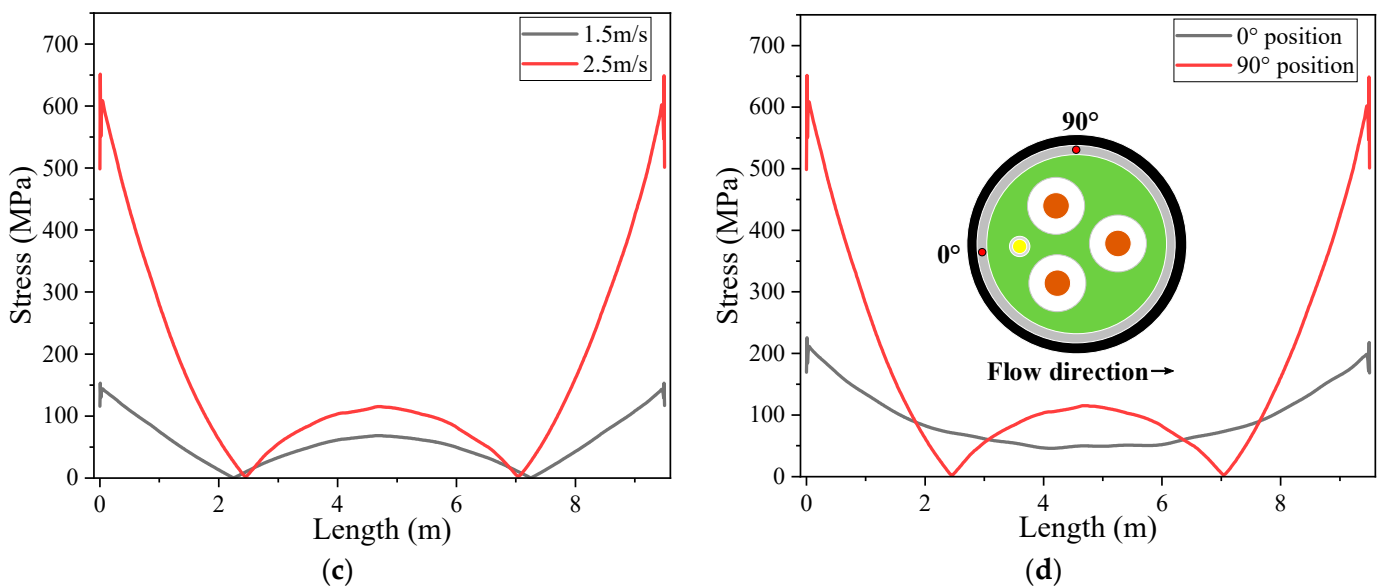


**Figure 8.** Stress analysis of the armor layer in submarine cable: (a) stress distribution nephogram of the armor layer at 1.5 m/s velocity, (b) stress distribution nephogram of the armor layer at 2.5 m/s velocity, (c) stress distribution curve of the armor layer under different flow velocities, and (d) stress distribution curve of the armor layer of different circumferential positions.

In addition, the stress distribution curves of different circumferential positions of the armor layer under the same velocity are extracted and shown in Figure 8d. It can be seen that the stress of the armor layer at 0° is smaller than that at 90°, and the distribution trend is gentler, while there is no peak at the middle position. On the contrary, the stress distribution at the 90° position significantly drops, and there are stress minimums near the 2.5 m and 7 m positions.

### 5.3. Simulation Results of Torsional Optical Fiber Stress Distribution Characteristics

Based on the simulation results, the stress distribution curve of the torsional optical fiber is shown in Figure 9. The different colored lines are corresponded to different moments in a vibration cycle. It can be seen that due to the torsional structure, the stress of the optical fiber is no longer symmetrically distributed along the length, and the maximum stress occurs alternately at both ends of the submarine cable with the vibration period. Under the vortex-induced vibration, the maximum stress peak appears near the position of 0 m at time 0, and the maximum stress peak appears near the position of 9.5 m at time 1/2 T. The stress distribution of the two cases approximately exhibits a mirror image relationship about the midpoint of the length. Only when the transverse vibration amplitude is zero, the stress of the torsional optical fiber is distributed approximately symmetrically along the length.

In addition, the fiber stress at each time alternates between large and small peaks along the length, and there are five more prominent peaks corresponding to the five periods of the optical fiber torsional pitch. Furthermore, these five significant peaks gradually decrease along the length when the transverse vibration amplitude is positive and gradually increase when the transverse vibration amplitude is negative. In terms of the time domain, within a vibration period, the change period of the fiber stress distribution is the same as the vibration period, that is, the frequency of the stress distribution change is the vortex-induced vibration frequency. Moreover, the position where the two adjacent stresses change the most can be regarded as the endpoints of the vortex-induced vibration suspension span.

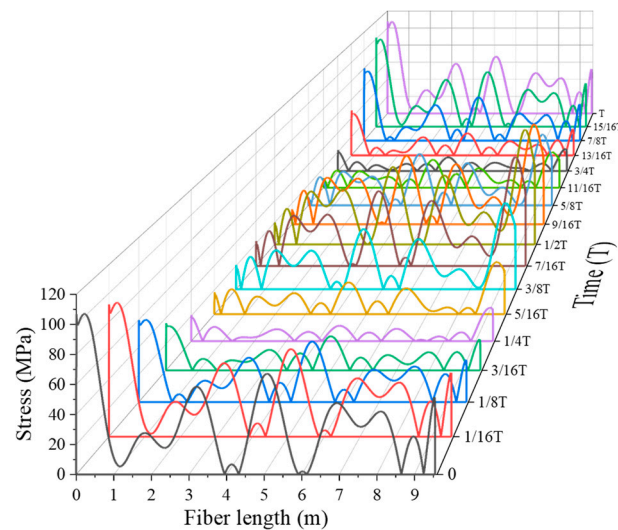


**Figure 9.** Length–time–stress distribution curve of torsional optical fiber position at 2.5 m/s flow velocity.

In addition, this study only analyzes the case where the water flow vertically scours a single section of a suspended span submarine cable. When the cable is subjected to scouring from different flow directions, there may be variations in the stress peaks at the starting and ending points of the vortex-induced vibration. If the submarine cable experiences vortex-induced vibrations in multiple suspended sections, different suspended spans can be distinguished by the frequency of vortex-induced vibration or stress change frequency, as well as the maximum position of stress change.

## 6. Conclusions

In this study, a fluid–structure coupling finite element simulation model is developed for the 35 kV three-core XLPE insulated optical fiber composite submarine cable. The natural frequency of the submarine cable model is simulated, and the vortex-induced vibration characteristics of the submarine cable under different flow velocities are analyzed. Then the time–frequency characteristics of the transverse vibration amplitude of the submarine cable during vortex-induced vibration are obtained. As well as the stress distribution characteristics of the armor layer and torsional optical fiber are obtained. According to the analysis, the following conclusions can be drawn.

1. The vortex-induced vibration frequencies of the submarine cable at the velocities of 1.5 m/s and 2.5 m/s are 2.44 Hz, 3.42 Hz, and 5.86 Hz. In addition, the former has the phenomenon of beat vibration, which is composed of two vibrations with similar frequencies, showing amplitudes that increase and decrease with time. Moreover, the latter has the phenomenon of locking after the reduced speed reaches 5.62, causing a rapid increase in the transverse vibrational amplitude.
2. The stress distribution and development law of the torsional optical fiber in the vortex-induced vibration of the three-core submarine cable is obtained. The stress distribution of the torsional optical fiber at time 0 and 1/2 T exhibits a mirror image relationship about the midpoint of the cable length. In addition, the frequency of the stress distribution change corresponds to the frequency of the vortex-induced vibration. In the monitoring of submarine cable operations, whether vortex-induced vibration occurs can be judged by the change in the stress distribution with regular frequency or vibration frequency. Additionally, according to the position of maximum stress change, the head and end of the vortex-induced vibration of the submarine cable can be judged, and the position and length of the vortex-induced vibration can be obtained. Moreover, experimental verification of the actual cables under simulated working conditions will be carried out in the future.

**Author Contributions:** Conceptualization, Y.H. and H.T.; methodology, H.T., P.Z. and Q.L.; software, H.T.; validation, H.T., L.C. and W.T.; writing—original draft preparation, H.T.; writing—review and editing, Y.H. and H.T.; supervision, Y.H., L.L. and L.Y. All authors have read and agreed to the published version of the manuscript.

**Funding:** This research was funded by the Smart Grid Joint Fund Key Project between the National Natural Science Foundation of China and the State Grid Corporation under grant number [U1766220].

**Institutional Review Board Statement:** Not applicable.

**Informed Consent Statement:** Not applicable.

**Data Availability Statement:** The data supporting the reported results cannot be shared at this time, as they have been used to produce more publications on this research.

**Acknowledgments:** This work is supported by the Smart Grid Joint Fund Key Project of the National Natural Science Foundation of China and State Grid Corporation (Grant No. U1766220).

**Conflicts of Interest:** The authors declare no conflict of interest.

## References

- Gulski, E.; Anders, G.J.; Jogen, R.A.; Parciak, J.; Siemiński, J.; Piesowicz, E.; Paszkiewicz, S.; Irska, I. Discussion of electrical and thermal aspects of offshore wind farms' power cables reliability. *Renew. Sustain. Energy Rev.* **2021**, *151*, 111580. [\[CrossRef\]](#)
- Aoife, F.; Paraic, H. The evolution of offshore wind power in the United Kingdom. *Renew. Sustain. Energy Rev.* **2014**, *37*, 599–612.
- Taormina, B.; Bald, J.; Want, A.; Thouzeau, G.; Lejart, M.; Desroy, N.; Carlier, A. A review of potential impacts of submarine power cables on the marine environment: Knowledge gaps, recommendations and future directions. *Renew. Sustain. Energy Rev.* **2018**, *96*, 380–391. [\[CrossRef\]](#)
- Ji, D.; Zhou, J.; Qian, J.; Shao, J.; Zhang, H. Current Development Review of Submarine Cable Detection Methods. *South. Power Syst. Technol.* **2021**, *15*, 36–49.
- Lv, A.; Kou, X.; Yin, C.; Li, Y. Modeling of Temperature Relation between Optical Fiber and Conductor in 3-Core Submarine Power Cable. *Trans. CES* **2016**, *31*, 59–65.
- Li, Q.; Hao, Y.; Zhang, P.; Tan, H.; Tian, W.; Chen, L.; Yang, L. Numerical Study of the Local Scouring Process and Influencing Factors of Semi-Exposed Submarine Cables. *J. Mar. Sci. Eng.* **2023**, *11*, 1349. [\[CrossRef\]](#)
- Guo, Q.; Wu, C.; Cen, Z.; Zhang, W.; Cai, C. Study on buried depth variation characteristics and causes of submarine cables at the west mouth of Qiongzhou Strait. *Sichuan Cem.* **2019**, *11*, 326+289.
- Chen, J.; Wu, C.; Chen, C.; Cen, Z.; Huang, X.; Zhang, W. Scouring mechanism and protective measures of buried submarine cables. *Chin. Offshore Plf.* **2020**, *35*, 68–73.
- Liu, G.; Li, H.; Qiu, Z.; Leng, D.; Li, Z.; Li, W. A mini review of recent progress on vortex-induced vibrations of marine risers. *Ocean Eng.* **2020**, *195*, 106704. [\[CrossRef\]](#)
- Raissi, M.; Wang, Z.; Triantafyllou, M.; Karniadakis, G. Deep learning of vortex-induced vibrations. *J. Fluid Mech.* **2019**, *861*, 119–137. [\[CrossRef\]](#)
- Zhao, L.; Li, Y.; Xu, Z.; Yang, Z.; Lü, A. On-line monitoring system of 110 kV submarine cable based on BOTDR. *Sens. Actuators A* **2014**, *216*, 28–35. [\[CrossRef\]](#)
- Lv, A.; Li, J. On-line monitoring system of 35 kV 3-core submarine power cable based on  $\phi$ -OTDR. *Sens. Actuators A* **2018**, *273*, 134–139. [\[CrossRef\]](#)
- Khodadadian, A.; Parvizi, M.; Abbaszadeh, M.; Dehghan, M.; Heitzinger, C. A multilevel Monte Carlo finite element method for the stochastic Cahn–Hilliard–Cook equation. *Comput. Mech.* **2019**, *64*, 937–949. [\[CrossRef\]](#) [\[PubMed\]](#)
- Noii, N.; Khodadadian, A.; Aldakheel, F. Probabilistic failure mechanisms via Monte Carlo simulations of complex microstructures. *Comput. Method Appl. Mech. Eng.* **2022**, *399*, 115358. [\[CrossRef\]](#)
- Tang, Y.; Fan, J.; Zhang, J.; Wang, L.; Gui, L. Analysis of longitudinal and transverse vortex induced vibration of a cylinder at high Reynolds number. *J. Vib. Shock* **2013**, *32*, 88–92.
- Xu, W.; Jia, K.; Ma, Y.; Wang, Y.; Song, Z. Multispan classification methods and interaction mechanism of submarine pipelines undergoing vortex-induced vibration. *Appl. Ocean Res.* **2022**, *120*, 103027. [\[CrossRef\]](#)
- Wu, X.; Ge, F.; Hong, Y. A review of recent studies on vortex-induced vibrations of long slender cylinders. *J. Fluid Struct.* **2012**, *28*, 292–308. [\[CrossRef\]](#)
- Pan, P.; Cai, B.; Tan, A.; Guo, Z.; Xie, S. Study on vortex induced vibration characteristics of submarine cables in sub main structures. *Ocean Eng.* **2015**, *33*, 45–51.
- Huang, X.; Zhang, Z.; Wang, S.; Wang, C.; Zhao, J.; Bian, Q.; Lv, A. Vortex Induced Vibration Analysis of 500kV Single-Core Optical Fiber Composed Submarine Power Cable Based on Finite Element Method. In Proceedings of the 2018 IEEE 3rd Advanced Information Technology, Electronic and Automation Control Conference (IAEAC), Chongqing, China, 12 October 2018; pp. 2287–2292.

20. Lv, A.; Pei, L. Fluid-Structure Coupled Finite Element Modeling Analysis of Vortex Induced Vibration Characteristics of Submarine Cable. *Comput. Simul.* **2022**, *39*, 89–94+277.
21. Derakhshandeh, J.; Alam, M. A review of bluff body wakes. *Ocean Eng.* **2019**, *182*, 475–488. [[CrossRef](#)]
22. Gustafsson, A. Analysis of Vortex-Induced Vibrations of Risers. Master's Thesis, Chalmers University of Technology, Gothenburg, Sweden, 2012.
23. Srinil, N.; Wiercigroch, M.; O'Brien, P. Reduced-order modelling of VIV of catenary riser. *Ocean Eng.* **2009**, *36*, 1404–1414. [[CrossRef](#)]
24. Hu, Y. Research on Modeling and Measurement Method of Vibration of Three-Core Submarine Cable Based on BOTDR. Master's Thesis, North China Electric Power University, Beijing, China, 2021.
25. Ibrahim, R. Friction-induced vibration, chatter, squeal, and chaos—Part II: Dynamics and modeling. *Appl. Mech. Rev.* **1994**, *47*, 227–253. [[CrossRef](#)]
26. Batchelor, G. *An Introduction to Fluid Dynamics*; Cambridge University Press: Cambridge, UK, 1967.
27. Zhou, W. Vortex Induced Vibration and Control of Offshore Pipelines Considering Three-Dimensional Full Field Fluid Structure Coupling. Master's Thesis, Zhejiang University, Hangzhou, China, 2018.

**Disclaimer/Publisher's Note:** The statements, opinions and data contained in all publications are solely those of the individual author(s) and contributor(s) and not of MDPI and/or the editor(s). MDPI and/or the editor(s) disclaim responsibility for any injury to people or property resulting from any ideas, methods, instructions or products referred to in the content.